Recycling of dredged sediment as a raw material for the manufacture of Portland cement – Numerical modeling of the hydration of synthesized cement using the CEMHYD3D code

Duc Chinh Chu, Joelle Kleib, Mouhamadou Amar, Mahfoud Benzerzour, Nor-Edine Abriak

Recycling of dredged sediment as a raw material for the manufacture of Portland cement – Numerical modeling of the hydration of synthesized cement using the CEMHYD3D code

Duc Chinh CHU[(1)(*)], Joelle KLEIB[(1)], Mouhamadou AMAR[(1)], Mahfoud BENZERZOUR[(1)], Nor-Edine ABRIAK[(1)]

[(1)] Univ.Lille, IMT Lille Douai, Univ.Artois, Yncrea Hauts-de-France, ULR 4515-LGCgE, 6 Laboratoire de Génie civil et géo-Environnement, F-59000, Lille, France

[(*)] **Corresponding author: Duc Chinh CHU**

Email: duc.chinh.chu@imt-lille-douai.fr

ABSTRACT

Around 56 million m^3 of sediments are dredged in France per year to maintain the access to ports and waterways. Sediments are considered as waste according regulations and cause environmental, ecological and economic issues. This paper aims to use dredged sediments as raw material to replace traditional materials in Portland cement production. Two cements were produced at the laboratory: a reference cement made from analytical grade reagents of $CaCO_3$, SiO_2, Al_2O_3 and Fe_2O_3 and a second cement made from sediment as a partial substitution for traditional materials. The components proportions in the raw meal were adjusted using the cementitious modulus values (LSF, SR and AR). The produced clinkers/cements were characterized by X-ray diffraction; X-ray fluorescence and scanning electron microscopy (SEM-EDS) in order to study their mineralogical and chemical composition as well as their microstructure. The reactivity of the cements was measured by isothermal calorimetry, and by the determination of the degree of hydration and the compressive strength. The CEMHYD3D code was used to numerically model the hydration of cement paste in order to follow the evolution of all phases and to predict the properties of hydrated cements.

The results demonstrate that sediments can be used as a raw material in the cement production at a high rate (31 wt%) without affecting the phase assemblage and the hydration behavior.

Keywords: Recycling, sediment, clinker, hydration, CEMHYD3D

Graphical abstract

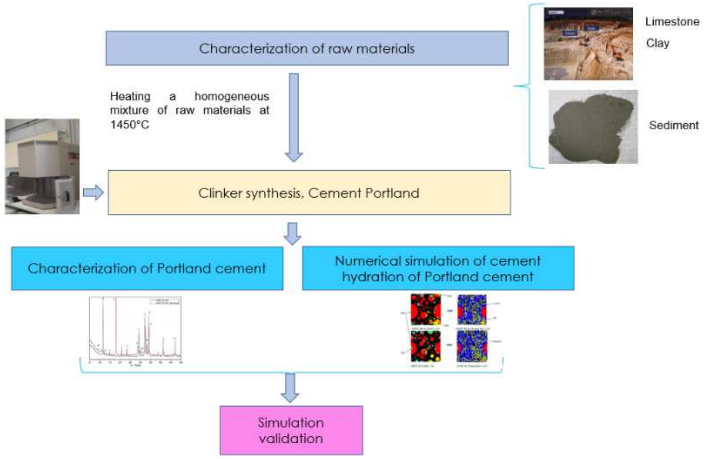

1. INTRODUCTION

In 2016, the French cement industry produced around 17 million tons of cement and was the leader in Portland cement production in the European Union [1]. However, the production of cement has a considerable impact on the environment related to the extraction of natural resources and CO_2 emissions [2]. In 2012, around 800 million tons of raw materials were extracted in France where 50% are allocated for the production of construction materials [3]. Consequently, the recycling of industrial by-products and waste as raw materials in the manufacture of cement has become a trend for reserving natural resources. Previous studies [4–9], have demonstrated the effectiveness of wastes use for a partial replacement of raw materials in the manufacture of cement.

In France, around 56 million m^3 of sediments (marine and river sediments) are dredged annually to restore acceptable navigation thresholds, to avoid flooding and to improve the quality of the environment. The sediments are either immersed in the sea, remained in the land (generally polluted sediment), or reused in various sectors such as construction materials and agriculture. Several treatment methods for sediments have been studied and

applied in various fields of civil engineering. Among these, the reuse of sediments in road construction as a base layer or a form layer [10–14], the manufacture of artificial aggregates [15], and as a mineral addition in mortars [16, 17]. In most of these applications, sediments should be treated before recycling.

In addition to the applications listed above, some studies have shown that sediments can replace a part of the raw materials used in cement production due to their chemical composition, which contains the principal oxides ($CaCO_3$, SiO_2, Al_2O_3, and Fe_2O_3) for clinker production. In fact, Portland cement contains approximately 95 wt% of clinker and 5 wt% of secondary constituents [18]. Portland clinker is made by burning at a high temperature (1450 °C) of a raw meal generally containing 80% limestone as a source of calcium oxide and 20% clay as a source of silica, alumina, and iron oxide. At high temperature, the chemical elements recombine to form four principal mineral phases such as : Alite (C_3S: $3CaO.SiO_2$), Belite (C_2S: $2CaO.SiO_2$), Tricalcium aluminate (C_3A: $3CaO.Al_2O_3$) and Alumino-tetracalcium ferrite (C_4AF: $4CaO.Al_2O_3.Fe_2O_3$) (Table 1) [18].

Table 1 Principal phases of clinker according to the cement nomenclature

Mineral phases	Cement nomenclature	Chemical formula	Minimum content (wt%)	Maximum content (wt%)
Alite	C_3S	Ca_3SiO_5	45.0	79.7
Belite	C_2S	Ca_2SiO_4	5.7	29.8
Tricalcium aluminate	C_3A	$Ca_3Al_2O_5$	1.1	14.9
Alumino-tetracalcium ferrite	C_4AF	$Ca_4Al_2Fe_2O_{10}$	2.0	16.5

Dalton et al. [19] have produced a clinker/cement on a laboratory and industrial scale, with raw materials extracted from quarries and contaminated sediment from the port of New Jersey (New York). Different formulations with variable substitution rates of sediment from 1 to 12 wt% were tested. The authors noted that the Alite/Belite ratio in the clinkers decreased when the sediment content in the clinker was greater than 6.5 wt%. The compressive strength of these cements was slightly lower than that of the reference Portland cement. Therefore, they conclude that cooling is necessary to prevent the decomposition of alite into belite and free lime.

Aouad et al [20] used the fraction of polluted sediment with particles size smaller than 2 mm from the Scarpe Canal, located in the industrial basin of the North of France, to produce clinker/cement in the laboratory with a 39.1 wt% substitution rate of sediment. The authors showed that the four mineral phases of the cement were obtained without the appearance of secondary phases. The compressive strength of the cement paste made from sediment was 20% higher than that of the reference cement paste (CEM I 52.5 N) at 56 days.

The fine fraction of sediments with a particle size smaller than 200 µm from French hydroelectric reservoirs has been used by Faure et al. [21], [22] as a raw material for Portland cement production. The sediments replaced all or a part of the silico-aluminous raw materials in the raw mixes. Portland cements made from clinkers containing 10 -15 wt% of sediments presented a high hydraulic reactivity and no constraints in terms of fresh state workability and shrinkage.

Therefore, the objectives of this study are, first to produce a clinker/cement at a laboratory with the maximal amount of sediment from the North of France. The cement made from substitution of sediment for the raw materials was characterized and compared to those produced from pure raw materials in order to study the substitution impacts of the sediment on the clinker/cement properties and the hydration behavior of cement paste. Second, the CEMHYD3D code was used to simulate numerically the hydration of the cement pastes over time. The experimental results were compared with the simulation results to validate the code. The simulation of cement hydration is interesting because it allows us to understand the hydration behavior and to follow the evolution of all phases over time.

2. MATERIALS AND RESEARCH METHOD

The raw materials used in this study for clinker/cement production are the analytical grade reagents of $CaCO_3$, SiO_2, Al_2O_3, Fe_2O_3, and sediment. The sediment used is river sediment collected from different points on the site located in Noyelles-Sous-Lens (noted NSL sediment) of the North of France. The sediment was homogenized and

dried at 40 °C to reach a constant weight, then grounded to reach a particle size smaller than 200 µm with a centrifugal ball mill.

2.1. Results of the sediment characterization

Different characterizations were conducted on the sediment before using it in the raw meal for clinker production.

The physical characterization consists of determining: the particle size distribution of the sediment measured by the laser particle analyzer COULTER type LS 13 320 , the organic matter content (OM) measured according to the XP P94-047 standard [23], the density determined using the helium pycnometer Accupyc 1330 type [24], the specific surface area of sediment measured by the Brunauer-Emmett-Teller (BET) method, and the Blaine method [25].

The chemical composition of the raw materials was identified using X-ray fluorescence analysis (XRF).

The mineralogy of the sediment was studied using the XRD analysis (XRD Bruker D2 Advance device equipped with Cu Kα radiation, λ = 1.5406 Å) with the angle acquired 2θ from 5° to 80° and a step size of 0.02. In order to complete the sediment's characterization, a thermogravimetric analysis TGA/DTA (Netzsch STA 409 device) was performed on dried fine sediment (particle size smaller than 40 µm) with a rate of 10 °C/min and temperature range from 40 °C to 1000 °C.

The mobility of the metallic trace elements (MTE) and the anionic elements of the sediment were measured after the leaching of the sample using a liquid/solid ratio of 10 and an equilibrium time of 24h according to the standard NF EN 12457-2 [26] using an Inductively Coupled Plasma Optical Emission Spectrometer (ICP-OES 5100 Agilent Technologies). The leaching limit values for inert waste (IW) and non-hazardous waste (NHW) specified in Directive 1999/31/EC were used to verify material compliance.

2.1.1. The physical characteristics of the sediment

The results of the physical characterization are shown in Table 2. The NSL sediment has an organic matter content of 16.1 wt%. The Blaine surface of the sediment is two times larger than that of Portland cement (with a value of 3800 cm^2/g). The BET surface of the sediment is higher than that of Blaine because it is more influenced by the roughness of the surface and the open porosity [18]. The value is five times larger than that of Portland cement (with a value of 9000 cm^2/g).

Table 2 Physical characteristics of the sediment

Physical characteristics	NSL
Density (g/cm^3)	2.43
BET (cm^2/g)	43 765
Blaine surface (cm^2/g)	6 562
OM content (wt%)	16.1
LOI 950°C (wt%)	27.63
d_{10} (µm)	1.39
d_{50} (µm)	10.16
d_{90} (µm)	47.90

The particle size distribution of the sediment presented in Fig. 1 shows that 99.7% of the particles are smaller than 200 µm. This result is in accordance with the particle size required for the raw materials in the cement industry [27].

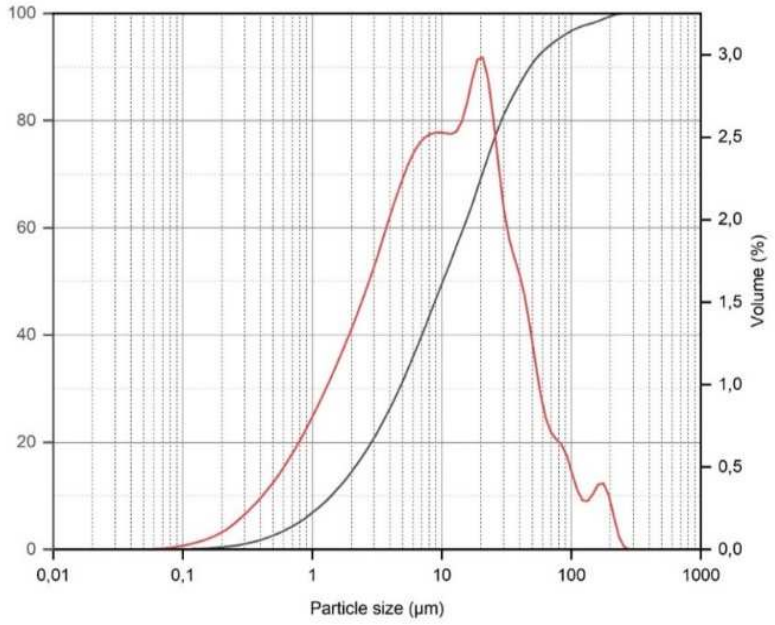

Fig. 1 Particle size distribution of the NSL sediment

2.1.2. Chemical and mineral characteristics

Table 3 shows the chemical composition of the sediment as well as of the other raw materials. The four principal oxides of the sediment are SiO_2, CaO, Al_2O_3 and Fe_2O_3. In addition, minor oxides such as MgO, ZnO, Na_2O and K_2O are detected, and their presence could have an impact on the clinker properties. The chemical composition shows that the content of 4 principal oxides ($CaO + SiO_2 + Al_2O_3 + Fe_2O_3$) of the calcined sediment is equal to 89.75% which is in accordance with the agreement between French cement industry groups signed in 2001 in order to define the limits of acceptability of the use of the mineral waste used as raw materials in the plant [28]. According to this agreement, calcined waste must comply with the following composition:

$$CaO + SiO_2 + Al_2O_3 + Fe_2O_3 \geq 80\%$$

Table 3 Chemical compositions of raw materials measured by XRF analysis

Oxides (wt%)	NSL	$CaCO_3$	Fe_2O_3	SiO_2	Al_2O_3
SiO_2	39.62	0	0	98.5	0
Al_2O_3	9.64	0	0	0.6	100
Fe_2O_3	5.12	0	96	0.1	0
CaO	10.57	55	0	0	0
MgO	0.88	0	0	0	-
Na_2O	0.69	0	0	0	-
K_2O	1.84	0	0	0	-
SO_3 total	0.22	0	0	0	-

TiO_2	0.60	0	0	0	-
P_2O_5	2.10	0	0	0	-
ZnO	0.27	0	0	0	-
L.O.I 950°C	27.63	45	0	0	-
Total (wt%)	99.17	100	96	99.2	100

The results of the mineral analysis (Fig. 2) show that the principal phases of the sediment are quartz (SiO_2), calcite ($CaCO_3$), brushite ($CaHPO_4.2H_2O$) and muscovite ($KAl_2(AlSi_3O_{10})(OH,F)_2$. These results are in accordance with previous studies conducted on the same sediment [10], [16], [21].

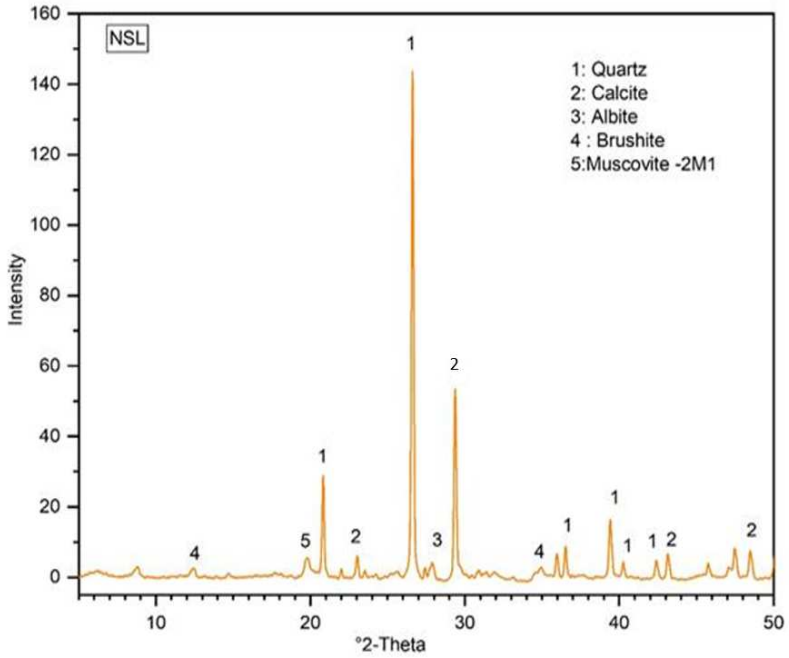

Fig. 2 X-ray diffraction (XRD) of the NSL sediment

The TGA - DTA analysis of NSL sediment (Fig. 3) shows three main peaks related to associated phenomena. The loss of mass between 212 °C and 550 °C is probably due to the combustion reactions of organic matter, organic pollutants (PAHs, PCBs, and TBT) [29], intergranular water, and constitution water from clay minerals [30] under the effect of temperature. A peak appears between 615 °C and 850 °C which corresponds mainly to the calcite decomposition. This result confirms that the presence of calcium oxide in the sediment is mainly in the form of calcite, corresponding to the result identified by XRD analysis. The results are summarized in Table 4.

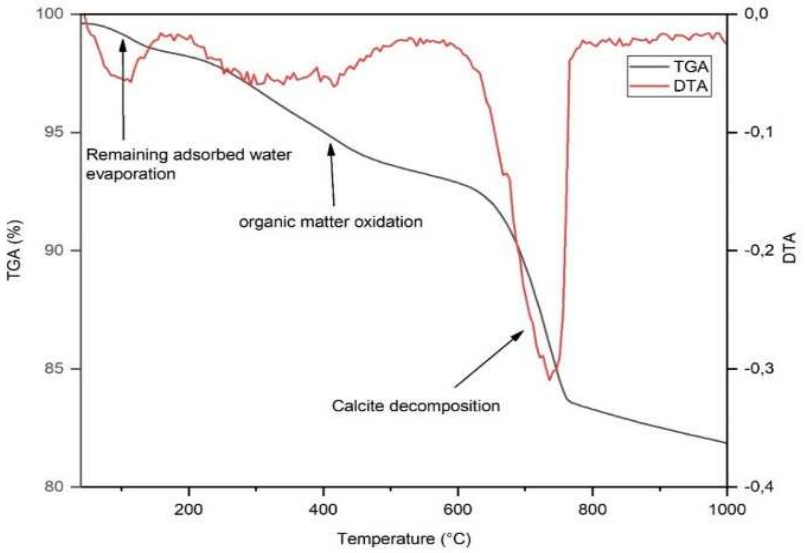

Fig. 3 TGA/DTA analysis of the NSL sediment

Table 4 Weight loss at different temperatures for NSL sediment

Temperature range (°C)	Weight loss (wt%)	Attributed reaction
105 °C – 150 °C	0.65	Remaining adsorbed water evaporation
212 °C – 550 °C	4.89	Organic matter, clay phase decomposition
615 °C – 850 °C	9.72	Calcite decomposition
40 °C – 1000 °C	17.74	Total weight loss

2.1.3. Environmental characteristics

The result of the leaching analysis shows the presence of metallic trace elements as well as anionic elements in the sediment (Table 5). The content of certain metallic trace elements in the NSL sediment exceeds the value specified for inert waste (IW), in particular, the Zn content. Nevertheless, these values are below the acceptable limits of heavy metals in the common agreement between the French cement industries [28].

Table 5 Metallic trace elements and anionic element's content in sediment (mg/kg)

Elements	**NSL**	**IW**	**NHW**
As (mg/kg)	< 0.08	**0.5**	**2**
Ba (mg/kg)	1.4912	**20**	**100**
Cd (mg/kg)	< 0.008	**0.04**	**1**
Cr (mg/kg)	< 0.03	**0.5**	**10**
Cu (mg/kg)	2.0509	**2**	**50**
Mo (mg/kg)	0.5538	**0.5**	**10**
Ni (mg/kg)	0.4799	**0.4**	**10**

Pb (mg/kg)	0.0447	**0.5**	**10**
Sb (mg/kg)	-	**0.06**	**0.7**
Se (mg/kg)	0.1019	**0.1**	**0.5**
Zn (mg/kg)	7.8518	**4**	**50**
Fluoride (mg/kg)	< 1	**10**	**150**
Chloride (mg/kg)	265	**800**	**15 000**
Sulfates (mg/kg)	15 820	**1000**	**20 000**

2.2. Clinker and cement synthesis method

From the result of the material's chemical composition, the different formulations of the raw meal were set up based on the following modulus usually used in the cement industry: the Lime Saturation Factor (LSF), the Silica Ratio (SR) and the Alumina Ratio (AR) [18]. These are the main parameters to control the quality of the clinker [31]. The calculations of LSF, SR, and AR are presented by the following equations:

$$LSF = \frac{100 * \%CaO}{2.8 * \%SiO2 + 1.18 * \%Al2O3 + 065 * \%Fe2O3} \quad \text{Eq(1)}$$

$$SR = \frac{\%SiO2}{\%Al2O3 + \%Fe2O3} \quad \text{Eq(2)}$$

$$AR = \frac{\%Al2O3}{\%Fe2O3} \quad \text{Eq(3)}$$

The LSF ensures good stoichiometry between calcium oxide and the other three main oxides. A higher LSF value corresponds to higher calcium silicate content, but the burning will be more difficult and may cause volume instability of the hydrated cement (high content of free lime). In addition, the LSF helps to control the relationship between the quantity of C_3S and C_2S [32]. The value of LSF is usually considered to be between 95 and 97 [33] but technically the range of LSF can vary from 90 to 104 [34].

The SR allows the determination of the relative proportion between the silicate phases and the aluminate phases. A high value of SR will cause difficulty in the clinkering process due to a lack of fluxing agents. This modulus also affects the clinker properties including the setting and durability. The value of SR is between 2.0 and 3.0 [18], but a more restrictive and optimized domain can be given between 2.4 and 2.6 [33].

Finally, the AR expresses the relative ratio in the interstitial phases between the C_3A and C_4AF phases. A high value of AR will provoke the formation of a high content of C_3A in the clinker and this affects the resistance to sulfates [35]. The appropriate AR value is between 1.5 and 1.8 [33].

From the chemical composition of each raw material, two different formulations of clinkers were formulated. The first is a reference clinker referred by CP 97TM produced using analytical grade reagents of $CaCO_3$, SiO_2, Fe_2O_3 and Al_2O_3 (without sediment) only. The second referred by CP97, was produced with a partial replacement of the raw material by the sediment. The modulus values applied to both clinkers are LSF = 97, SR = 2.6 and AR = 1.45. The choice of value LSF = 97 is to avoid the significant presence of CaO_{free} and to have a significant content of C_3S in the clinker. The solver option in Microsoft Excel was used to adjust and calculate the amount of the each raw material in the formulation while respecting the values of the targeted modulus. Table 6 shows the mixes designs of the two clinker raw meals.

Table 6 Mixes designs for the two produced clinker raw meals

Constituents	NSL (wt%)	$CaCO_3$ (wt%)	Al_2O_3 (wt%)	Fe_2O_3 (wt%)	SiO_2 (wt%)
CP 97 TM	0	79.99	3.17	2.32	14.52

CP 97	31	67.61	0	0.5	0.89

To prepare the raw mixes, all materials were first mixed by adding water with a water/material ratio = 0.6 to better homogenize. After drying at 105 °C, the pellets (with a diameter = 40 mm and a height = 15 mm) were produced using a press at 5 KN to obtain a more regular clinkering process. The pellets were burned at 200 °C for 20 minutes, then to 1450 °C with a rate of 7 °C/minute. After 15 min of burning at the clinkering temperature, the clinker was slowly cooled in the furnace. The clinker was ground to a Blaine specific surface of 3500 cm^2/g. Finally, the cements were obtained by mixing pure gypsum ($CaSO_4.2H_2O$) with clinker. The addition of gypsum has a very important role in controlling the setting of the cement. Indeed, the reaction of C_3A with water is very violent and immediately stiffens the cement paste [36]. This phenomenon is due to the formation of hydrated calcium aluminates according to Eq(4), which are distributed in the space filled with the mixing water and constitute bridges between the particles of the cement causing a rapid setting.

$$C_3A + 21H \rightarrow C_2AH_8 + C_4AH_{13} \rightarrow C_3AH_6 \quad \text{Eq(4)}$$

In addition, the presence of sulfate increases the hydration of C_3S, which requires an improvement in the development of compressive strength [37] and stability control of the volume of the paste [18]. However, an excess of sulfate can cause swelling by the late reaction with tricalcium aluminate [38], which increases the rate of degradation and deterioration of concrete [39]. The limit content of SO_3 is set at 3.5 wt% by the standard EN 197-1 [40]. Based on Day's hypothesis which assumed that the ettringite's formation would be delayed for a SO_3/Al_2O_3 ratio greater than 0.7. In this study, gypsum was added to reach an SO_3/Al_2O_3 ratio of 0.6. Table 7 shows the proportions of the constituents of the two cements.

Table 7 Mixes design of the OPC 97 TM and OPC 97 cement

Component	OPC 97 TM	OPC 97
Clinker (wt%)	95.67	95.16
Gypsum (wt%)	4.33	4.84

2.3. Clinkers/Cements characterization method

The chemical composition of raw meals, clinkers and cements measured by XRF analysis allows us to verify the values of the modulus used.

The mineralogy of the clinkers, cements and cement pastes was studied by XRD analysis using XRD Bruker D2 Advance device equipped with Cu Kα radiation, λ = 1.5406 Å. The polymorphs of crystalline phases of clinkers were studied in detail to understand the influence of the substitution of sediment on the formation of crystalline phases. The Bogue's formula [7] was used to quantify the crystalline phases of the clinker according to the following equations (Eq(5) -> Eq(8)) :

$$C_3S = 4.07 * (CaO_{Total} - CaO_{free\ lime}) - 6.72 * Al_2O_3 - 1.43 * Fe_2O_3 \quad \text{Eq(5)}$$

$$C_2S = 8.60 * SiO_2 + 1.08 * Fe_2O_3 + 5.07 * Al_2O_3 - 3.07 * (CaO_{Total} - CaO_{free\ lime}) \quad \text{Eq(6)}$$

$$C_3A = 2.65 * Al_2O_3 - 1.69 * Fe_2O_3 \quad \text{Eq(7)}$$

$$C_4AF = 3.04 * Fe_2O_3 \quad \text{Eq(8)}$$

The free lime content of the clinker is an important parameter to evaluate the quality of the clinkering process. In general, a free lime content less than 2 wt% is acceptable in the cement industry [41]. In this study, the free lime content of the clinker was determined according to the Schlafer-Bukokowski method.

To observe the effect of the substitution of sediment on the form of crystalline phases, the optical microscope was used to study the microstructure of clinker.

The chemical composition of the clinker phases was studied on polished sections with a Hitachi S-4300 SE/N scanning electron microscope operating in backscattered electron mode (20 keV) and equipped with an energy

dispersive X-ray spectrometer (EDS). To make the polished section, the clinker sample was vacuum impregnated in epoxy resin and polished down to 1 µm with ethanol to avoid reaction with water. Finally, the sample was coated with carbon before observation. About 50 points were measured for each crystalline phases of clinker on several zones.

The hydration reactions of the cement paste are exothermic and can be followed by measuring the rate of heat release. Therefore, the reactivity of the cements was followed using the isothermal calorimetry measurements performed at 20 °C. Based on a previous study [42], 8 g of cement and 4 g of water previously stored at 20 °C were mixed manually for two minutes before introduction in cells that were placed inside the calorimeter. The calorimeter was a home-made calorimeter using fluxmeters the allowed the calorimeter to equilibrate in less than 5 min.

The reactivity of the cements was also investigated by the measurement of the degree of cement paste hydration. In the literature, several methods were used to determine the degree of hydration of cement such as:

- Scanning electron microscopy (SEM-BSE) [43]
- Thermogravimetric analysis (TGA) [43]
- X-ray diffraction (XRD)
- Compressive strength

In a previous study, CHU et al [43] determined the degree of hydration of Portland cement by three different methods. The result shows that the bound water quantification method gave the most reasonable result. In this study, the degree of hydration of cement paste was determined by the bound water quantification method using TGA analysis. To prepare the cement paste, cement and water were manually mixed for 3 minutes with a W/C ration equal to 0.5. The paste was introduced into moulds and kept for 24h at 100% relative humidity at 20 °C. The sample was demoulded after 24h and stored in saturated lime solution at 20 °C to avoid the carbonation phenomenon before measurement at 2 and 28 days. The relative humidity of conservation considerably modifies the kinetics of hydration of the cementitious material. In fact, the hydration of CEM I cement is greatly reduced when the internal relative humidity passes below 80% [44]. Snyder et al. [45] showed that internal humidity was influenced by external relative humidity and the degree of hydration of the sample stored in the endogenous condition was lower than that of the sample stored in a saturated environment. For this reason, in this study, the curing was performed at 100% relative humidity.

The degree of hydration of the cement paste was determined according to the following equation:

$$\alpha(t) = \frac{Wn\,(t)}{Wn(\infty)} \qquad \text{Eq(9)}$$

With:

$\alpha(t)$: Degree of hydration of the sample at time t.

$W_n(t)$: Amount of bound water at time t (in gram of water per 100 g of anhydrous cement).

$W_n(\infty)$: Amount of bound water for a complete hydration of the cement paste (in gram of water per 100 g of anhydrous cement).

The value of $W_n(t)$ can be determined experimentally using the equation Eq(10) if the two following conditions are met:

- No carbonation in the cement paste.
- Low weight loss of anhydrous cement before 1000 °C

$$W_n(t) = \frac{\Delta m\ sample\ (105\ °C - 1000\ °C)(t)}{m\ sample\ (1000°C)(t)} * 100 \qquad \text{Eq(10)}$$

To determine the value of $W_n(\infty)$, NIST (National Institute of Standards and Technology) provides an approximate theoretical estimation of the amount of bound water produced for the five principal mineral phases of cement when the hydration is complete [46] (Table 12). In addition, in this study, no method for arresting for hydration of cement was used to avoid the carbonation phenomenon in the cement paste. The cement paste for the TGA analysis was immediately analyzed after reaching the desired hydration time (2 and 28 days) using the NETZSCH STA 409 type device according to the following condition: the temperature was increased from 30 °C to 105 °C with a rate of 2 °C/min, then maintained at 105 °C for 1h before increasing to the 1100 °C with a rate of 3 °C/min.

The compressive strength is measured to evaluate the quality and the mechanical performance of the produced cement. Due to limited quantities of the produced cement at laboratory (about 150 g), the compressive strength was determined on small cubes of dimension 1 x 1 x 1 cm^3 made from the cement paste with a W/C ratio equal to 0.5. The preparation process of the cement paste in this part is similar to that in the analysis of the degree of hydration. Based on previous studies [20, 43, 47], the compressive strength was measured on 6 samples after 2, 15 and 28 days performing at a constant stress of 0.3 MPa/s.

2.4. Numerical modeling of cement hydration using the CEMHYD3D code

2.4.1. CEMHYD3D code

The hydration of cementitious materials is a complex physicochemical process. Consequently, a numerical simulation of this process is very useful to know the state of the material as well as to follow the evolution of the phases in the hydration time. There are four main models for modeling cementitious materials hydration in the literature:

- Analytical models [48]
- Semi – analytical models [49]
- Thermodynamic models [50]
- Models associated with the development of microstructure (CEMHYD3D, HYMOSTRUC [51])

The semi-analytical model gives the degree of hydration of the cement from the degree of hydration of each phase of the clinker according to the following equation:

$$\alpha(t) = \alpha_{C3S}(t) * [\%C_3S] + \alpha_{C2S}(t) * [\%C_2S] + \alpha_{C3A}(t) * [\%C3A] + \alpha_{C4AF}(t) * [\%C_4AF] \quad \text{Eq(11)}$$

With:

α (t): Degree of hydration of the cement at time t.

α_{C3S} (t), α_{C2S} (t), α_{C3A} (t), α_{C4AF} (t): Degree of hydration of C_3S, C_2S, C_3A and C_4AF respectively at time t.

[%C_3S], [%C_2S], [%C_3A], [%C_4AF]: Initial mass proportion of C_3S, C_2S, C_3A and C_4AF respectively in the cement.

However, it is difficult to determine the degree of hydration of each phase in this case. Therefore, this model is not suitable to simulate the hydration of cement in this study.

The CEMHYD3D code developed by P.Bentz at NIST has been used successfully in several previous studies [52],[53],[54]. It allows the user to numerically generate and hydrate a 3D - microstructure of the cement paste made from the data input such as : the mineral composition, the particle size distribution and W/C volume ratio, under controlled hydration conditions [55]. The code does not use a classical chemical equations with the equilibrium of species in solution and the resolution of the associated equations systems, but instead uses a completely original mechanism of reaction between species using cellular automata [56]. A list of the chemical equations taken into account to perform the hydration of the numerical cement is detailed by P.Benzt in the CEMHYD3D user guide [57]. A 3D microstructure consists of micro cubes of dimension of 1 μm^3, called voxels, each representing a phase for example: solid (C_3S, C_2S, C_3A, C_4AF, gypsum, hydrates etc.), liquid (water). The advantage of the CEMHYD3D code is to allow the user to access to all the information such as the amount and the evolution of all phases, the porosity and the mechanical resistance of the hydrated cement paste over time. The microstructure generated from CEMHYD3D code could be used to study the leaching, the interfacial transition zone (ITZ) properties of the cementitious material [58, 59]. However, the porosity of the microstructure measured in the CEMHYD3D code is limited to the capillary porosity due to the size of the voxels equal to 1 μm^3 which is larger than the pore size in the hydrated cement paste.

The compressive strength in the model is estimated using Powers's empirical relation [57] according to the following equation :

$$\sigma_c(t) = \sigma_0(X(t))^n \quad \text{Eq(12)}$$

With:

σ_c(t): Compressive strength of sample at time t.

σ_0: Compressive strength of sample when capillary porosity is equal to 0. It is calibrated from the experimental resistance measured at 28 days.

n: Value is between 2.6 and 3.0. In general, a value equal to 2.6 is applied for CEM I.

X(t): Ratio of hydrate gel-space. In the CEMHYD3D code, X(t) is determined according to the following equation:

$$X(t) = \frac{Number\ of\ hydrate\ pixels}{Number\ of\ hydrate\ pixels + Number\ of\ porosity\ pixels} \quad \text{Eq(13)}$$

We also have:

$$X(t) = \frac{0.68\ \alpha(t)}{0.32\alpha(t) + \frac{W}{C}} \quad \text{Eq(14)}$$

With:

α(t): Degree of hydration of sample at time t.

W/C: water/cement ratio

2.4.2. Determination of time constant

The time constant (β) is used to convert times/cycles in the CEMHYD3D code. The value should be determined experimentally by the user depending on the type of cement used. The relationship between time and the number of cycles is according to the following equation:

$$t = \frac{\beta}{K} * c^2 \quad \text{Eq(15)}$$

With:

t: Time of hydration in hours.

c: Number of hydration cycles performed by the program in the CEMHYD3D

β: Conversation factor cycles/time in hour/(cycles)^2.

K: Speed coefficient for the cycle.

The value of K is determined according to the following equation:

$$K = e^{\frac{E}{8.314}\left(\frac{1}{298.15} - \frac{1}{T°+273.15}\right)} \quad \text{Eq(16)}$$

With:

E: Activation energy of the cement in KJ/mol.

T°: Temperature of the system in °C.

To determine the β value, the degree of hydration of the cement paste should be used. The value of the coefficient K is calculated according to Eq(16) equation with the activation energy of the cement E = 40 (KJ/mol) and gives a result of K = 0.9997. Knowing the experimental value of the degree of hydration of the cement paste at a given time, the user determines the number of hydration cycles for which the program reaches the same value as the experimental α(t) [56].

3. RESULTS AND DISCUSSIONS

3.1. Clinker characterization

3.1.1. Mineral and chemical composition of CP 97 TM and CP 97 clinker

The chemical composition (before sintering) of the two formulations (CP 97TM and CP 97) was analyzed by XRF analysis in order to verify experimental content of principal oxides (Table 8).

Table 8 Chemical composition of CP 97TM and CP 97 raw meals measured by XRF analysis

Oxide (wt%)	CP 97 TM		CP 97	
	Theoretical	Experimental	Theoretical	Experimental
SiO_2	14.30	13.8	13.19	12.9
Al_2O_3	3.26	2.8	3.00	3.05
Fe_2O_3	2.25	2.1	2.07	2.07
CaO	43.99	43.8	40.58	40.26
MgO	0.00	0.00	0.27	0.33

Na_2O	0.00	0.00	0.21	Traces
K_2O	0.00	0.00	0.57	0.59
SO_3 total	0.00	0.00	0.07	0.12
TiO_2	0.00	0.00	0.19	0.17
P_2O_5	0.00	0.00	0.65	0.56
ZnO	0.00	0.00	0.08	0.1
LOI 950°C (wt%)	35.99	36.88	39.10	39.4
Total (%)	99.79	99.38	100.00	99.55
LSF	97.00	101.1	97.00	98.04
SR	2.60	2.81	2.60	2.52
AR	1.45	1.33	1.45	1.47
CaO/SiO_2	3.08	3.17	3.08	3.12

The experimental result was compared to the theoretical value in order to check the values of the modules used. A good compatibility was observed in particular in the case of the CP 97 formulation between the experimental and theoretical composition. However, an increase of LSF value in the case of the CP 97 TM formulation was noted. The result shows the presence of minor elements such as ZnO, SO_3, and MgO in the CP 97 formulation. These elements could have an effect on the formation of the clinker phases. Indeed, the presence of MgO promotes the formation of C_3S in the M1 polymorph. In contrast, the presence of SO_3 promotes the formation of C_3S in the M3 polymorph which is less reactive than the M1 polymorph [60]. In a previous study, Gineys et al. [61] showed that Zn affected the formation of C_3A. A decrease in C_3A content was observed when the Zn content was higher than 0.7 wt%.

The free lime content of two clinkers CP 97 TM and CP 97 corresponds to 1.287 wt% and 0.786 wt% respectively. The values are obviously below the acceptable threshold for free lime content in the cement industry (2 wt%). The result confirms that the clinkering was complete. Table 9 shows the mineralogical compositions according to the Bogue formula of two clinkers after sintering.

Table 9 Mineral composition of two clinkers CP 97TM and CP 97 measured by the Bogue's formula

Mineral phases (wt%)	CP 97TM	CP 97
C_3S	76.83	66.99
C_2S	4.96	10.69
C_3A	6.16	7.59
C_4AF	10.15	10.41
CaO free	1.287	0.786

To study the mineralogical assemblage of the two clinkers, XRD analysis was performed on the clinker powders. The XRD pattern represented in the Fig. 4 shows the presence of the four principal crystalline phases of clinker such as C_3S, C_2S, C_3A and C_4AF as well as the presence of free lime which was also determined according to the Schlafer-Bukokowski method. In addition, the result also indicates that no secondary mineral phase are identified in the CP 97 clinker and the major crystalline phases in the CP 97TM clinker are all present in the CP 97 clinker.

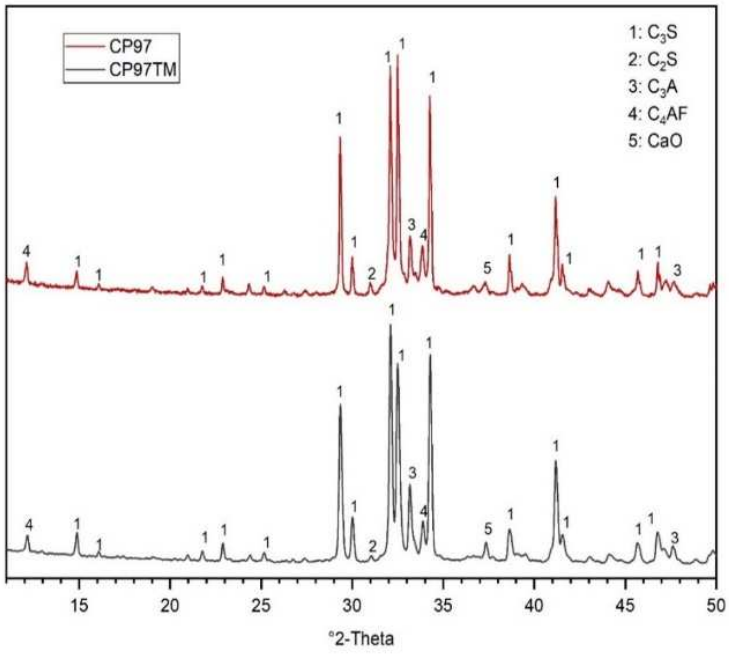

Fig. 4 X-ray diffraction (XRD) of the CP 97 TM and CP 97 clinker

The XRD pattern was examined at various ranges to study the effects of the substitution rate of the sediment in the raw materials on the polymorph of the crystalline phases formed in the clinker (Table 10).

Table 10 The angular range 2θ for the different mineral phases of clinker

Mineral phases	C_3S	C_2S	C_3A
2θ	[36°-38°]	[30.5°-32°]	[47°-48°]
	[55.5°-57.5°]	[32.7°-33.7°]	

We note that the XRD pattern curve of the CP 97TM clinker is more "smooth" than that of the CP 97 clinker. This may be due to the purity of the raw mix of CP 97 TM formulation which does not contain minor oxides. Concerning the polymorph of C_3S in the clinker, the XRD pattern presented in the Fig. 5 indicated the formation of the M1 and M3 polymorph in the CP 97 clinker whilst the M3 polymorph was not identified in the CP 97TM clinker.

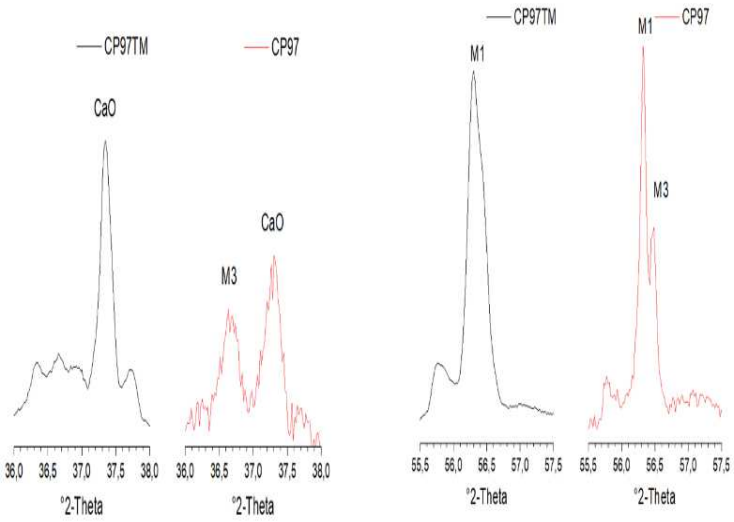

Fig. 5 M1 and M3 polymorph of C_3S of the clinker CP 97 TM and CP 97

To study the C_2S polymorph, the result presented in Fig. 6 shows that the incorporation of sediment in the raw meal did not affect the formation of C_2S. The result also shows that the β-C_2S polymorph is the principal polymorph of C_2S in the two clinkers. In addition, the result confirms that the cooling process in this study does not cause the decomposition of C_3S into ϒ-C_2S polymorph and CaO_{free} in the clinker. The decomposition of C_3S directly influences the quality of the cement because the ϒ-C_2S polymorph is much less reactive than C_3S, and this causes a decrease in C-S-H content which is the principal hydrate and contributes significantly to the macro – properties of concrete such as strength and durability [62, 63].

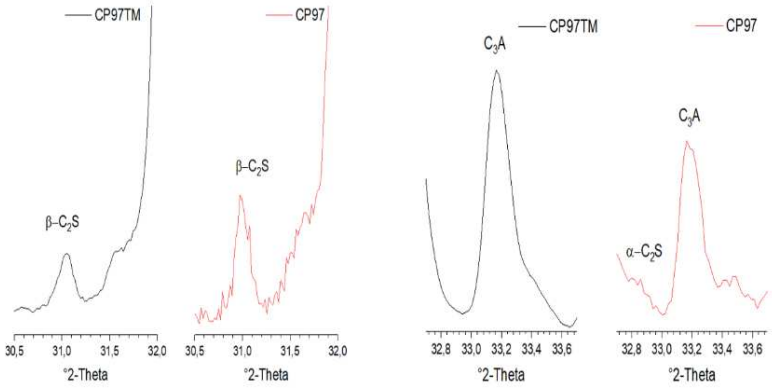

Fig. 6 β-C_2S and α-C_2S polymorph of the CP 97 TM and CP 97 clinker

The formation of orthorhombic polymorph of C_3A (Fig. 7) was observed in the CP 97 clinker. This could be due to the presence of Na^+ ions which replaced Ca^{2+} ions and led to the change from the cubic system to the orthorhombic system [64].

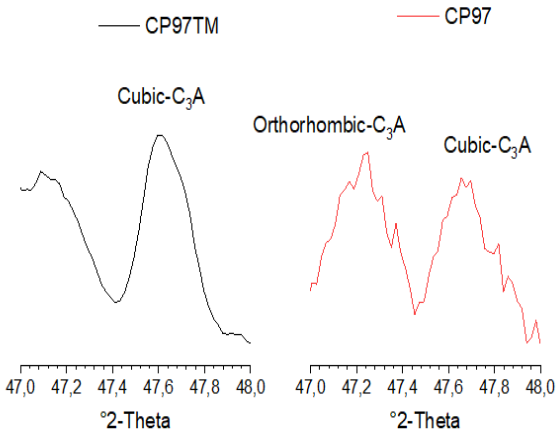

Fig. 7 Polymorph of C_3A phase of the CP 97 TM and CP 97 clinker

Fig.8 shows the polished sections of CP 97 TM and CP 97 clinkers observed by optical microscopy.

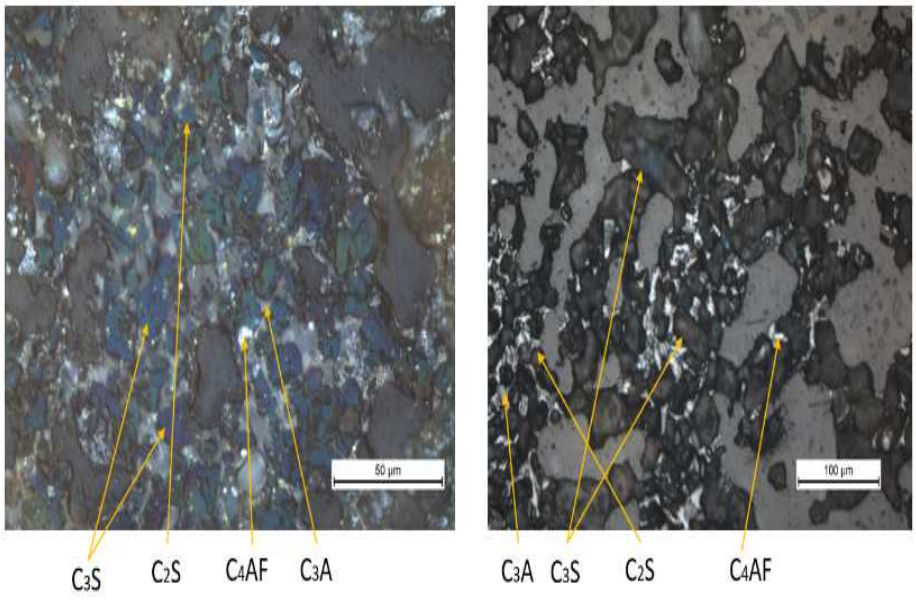

Fig. 8 Observation by optical microscope on the polished section of CP 97 TM (left) and CP 97 (right) clinker

A good distribution of silicate phases (C_3S and C_2S) and interstitial phases (C_3A and C_4AF) in the two clinkers was observed. The alite grains appeared to be angular whereas the belite is round. In addition, the presence of sulfate (SO_3) in the CP 97 clinker reduces the viscosity and surface tension of the interstitial liquid phase, and promotes the formation of alite crystals larger than those of reference clinker [65]. The result confirms that the substitution of sediment for traditional raw materials did not show any modification of distribution and form of the principal crystalline phases.

3.1.2. Chemical composition of mineral phases of clinkers (SEM-EDS analysis)

Fig. 9 and Fig. 10 show the result of the SEM – EDS analysis performed on the silicate phases of the CP 97 TM and CP 97 clinker.

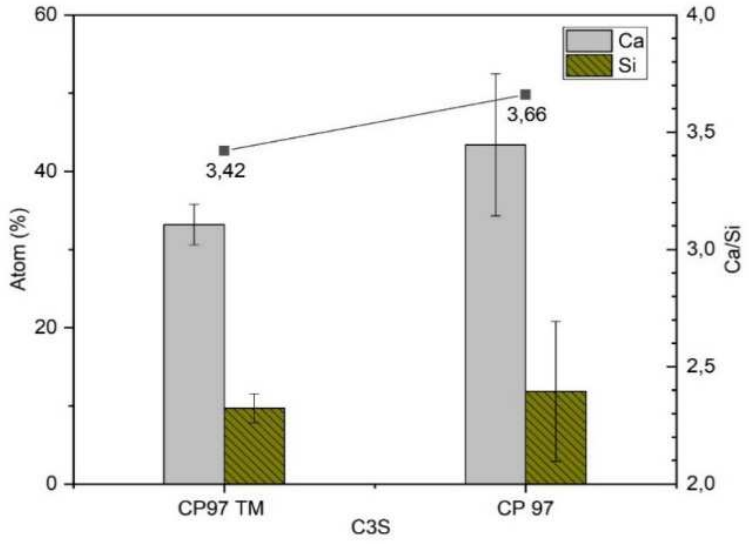

Fig. 9 Chemical composition and the ratio of major elements of C_3S phase

The result of the measurement of the C_3S phase shows that:

- The major elements of this phase identified are Ca, Si and O. The C/S (CaO/SiO_2) ratio measured by SEM – EDS analysis is higher than the theoretical value (C/S = 3) in the two clinkers This difference can be due to the points measured and to the size of the diffusion bulb which analyzes an area and not a point [66]. In addition, this ratio of CP 97 clinker is higher than that of CP 97 TM clinker.

- The minor elements incorporated in this phase are Al, Fe for CP 97 TM clinker and Al, Fe, Mg, alkali (Na, K) for CP 97 clinker. The Al/Si ratio is equal to 0.07 for the two clinkers. This value is higher than that in the Taylor's study which gave a Al/Si ratio equal to 0.04. The presence of Mg identified in this phase of the CP 97 clinker is in accordance with than previously observed by XRD analysis which shows the incorporation of Mg promotes the formation of M3 polymorph of the C_3S phase (Fig. 5).
- This phase of the CP 97 TM and CP 97 clinkers contains 1.14 wt% and 2 wt% of the minor elements respectively.

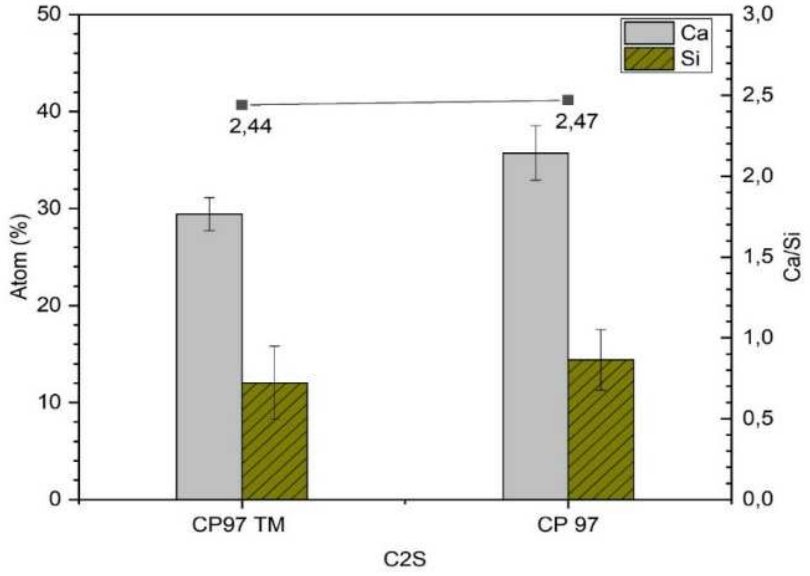

Fig. 10 Chemical composition and the ratio of major elements of C_2S phase

The result of the SEM - EDS analysis of the C_2S phase shows the following:

- The major elements of this phase also are Ca, Si and O. In addition, the C/S ratio of the two clinkers is higher than the theoretical value of the C_2S phase (C/S = 2). However, this ration is similar for the two clinkers.
- Same as the C_3S phase, the C_2S phase contains the minor elements such as Al, Fe in the CP 97 TM clinker and Al, Fe, Mg, alkali (Na, K) in the CP 97 clinker. The Al/Si ratio is equal to 0.07 for the two clinkers and this value is relatively similar to that in the Taylor's study (Al/Si = 0.077).
- The C_2S phase of the CP 97TM and CP 97 clinkers incorporates 1.42 wt% and 3.03 wt% of the minor elements respectively.

The result of the SEM - EDS analysis performed on the C_3S and C_2S phases shows that the substitution of sediment for the raw materials does not affect the ratio of major elements of the C_2S phase whilst it considerably affects the ratio of major elements of the phase C_3S. This is interesting because the C_3S phase contributes considerably to the hydration behavior and the mechanical performance of Portland cement.

Fig. 11 and Fig. 12 show the results of the SEM - EDS analysis at the interstitial crystalline phases.

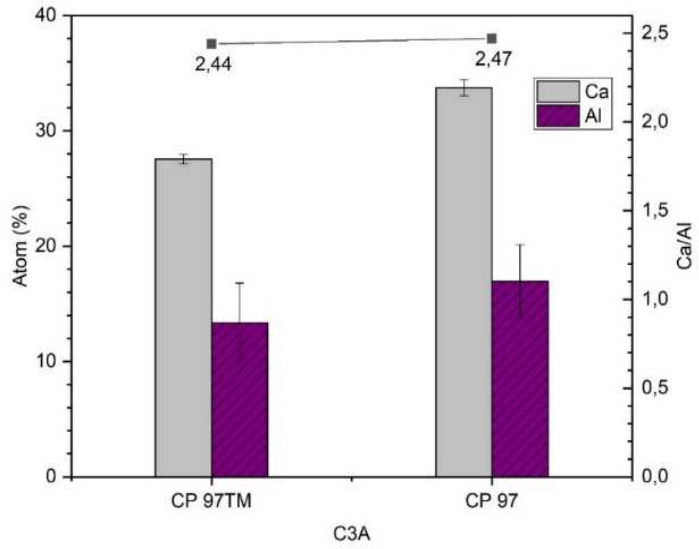

Fig. 11 Chemical composition and the ratio of the major elements of C_3A phase

From the result illustrated in Fig. 11, some conclusions can be made:

- The major elements identified in the C_3A phase are Ca, Al and O. The C/A (CaO/Al_2O_3) ratio in the two clinkers is higher than the theoretical value (Ca/Al = 1.5) of this phase. However, this ratio is relatively similar for the two clinkers.
- The C_3A phase contains the minor elements such as Fe, Si in the CP 97 TM clinker and Si, Fe, Mg, alkali (Na, K) in the CP 97 clinker. However, the amount of Mg incorporated into this phase is 10 times less than that in the C_3S phase.
- The presence of alkali (Na, K) identified in this phase of the CP 97 clinker is in accordance with than previously observed by XRD analysis which shows the incorporation of alkali promotes the formation of orthorhombic polymorph of C_3A phase (Fig. 7). The amount of alkali in this phase of the CP 97 clinker is five higher than that of the C_3S phase.
- The C_3A phase of the CP 97 TM and CP 97 clinkers incorporates 3.42 wt% and 4.55 wt% of the minor elements respectively.

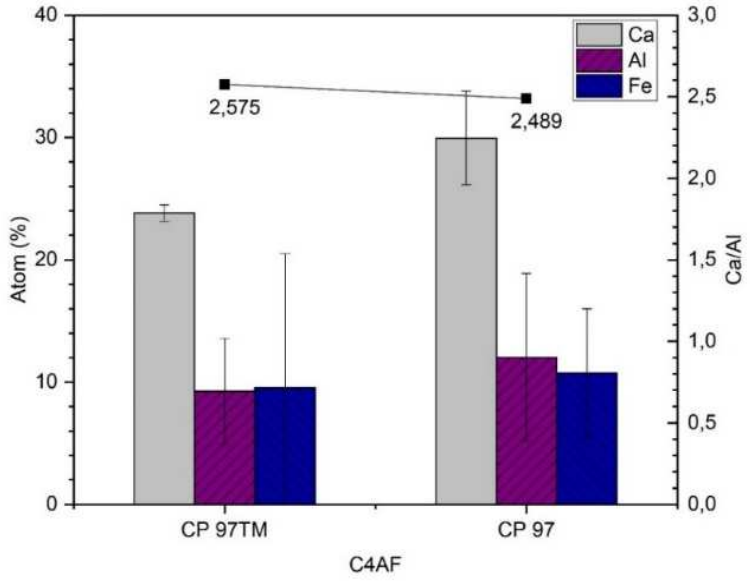

Fig. 12 Chemical composition and the ratio of the major elements of the C_4AF phase

The result of the SEM-EDS analysis of the phase C_4AF (Fig. 12) shows that:

- The major elements of this phase are Ca, Al, Fe and O. The Ca/Al (CaO/Al_2O_3) ratio in the two clinkers is higher than the theoretical value of this phase (Ca/Al = 2). However, this ration is similar in the two clinkers.
- In addition, the Al/Fe ratio is equal to 0.99 for CP 97TM clinker and equal to 1.12 for CP 97 clinker, which is relatively close to the theoretical value (Al/Fe = 1) of this phase.

The zinc is well known to have a retardation effect on the cement paste hydration [67]. Therefore, the determination of the location of zinc in the clinker phases is important in order to understand the effect of this element on the hydration behavior of cement. The result of the SEM – EDS analysis performed on the CP 97 clinker shows that Zn is present in all the clinker phases except in the C_2S phase (0.16 wt% in C_3S phase, 0.33 wt% in C_3A phase and 0.83 wt% in C_4AF phase). This result is in accordance with that previously observed [67]. In a previous study, Hornain also indicated that it is difficult for zinc to enter into C_2S phase [68].

3.2. CEMENT CHARACTERIZATION

3.2.1. Chemical composition of cements

The chemical composition of the two cements measured by XRF analysis is presented in Table 11. The result shows that the chemical composition of the principal oxides of OPC 97 cement is comparable to that of OPC 97 TM cement. However, it is important to note that the amount of zinc in OPC 97 is 10 times higher than that in Ordinary Portland Cement [20].

Table 11 Chemical composition of the OPC 97 TM, OPC97 cements measured by XRF analysis

Oxides (wt%)	OPC 97 TM	OPC 97
SiO_2	20.5	19.7
Al_2O_3	4.7	5
Fe_2O_3	3.1	3.1
CaO	65.5	62.4
MgO	ND	0.6
Na_2O	ND	ND
K_2O	ND	0.5
SO_3	1.9	2.5
TiO_2	ND	0.3
P_2O_5	ND	0.9
ZnO	ND	0.2
L.O.I	3.6	4.0
Total (%)	99.2	99.0

3.2.2. Heat of cement hydration

The rates of heat evolution of the hydrated cement pastes are shown in Fig. 13. The result indicates that the OPC 97 cement presents hydration behavior similar to the OPC 97 TM because the curve shapes are similar. By comparing the two curves, we also note that the setting of OPC 97 TM begins before OPC 97 cement (point 1). This could be due to the higher reactivity of the M1 polymorph compared to the M3 polymorph in C_3S phase. Indeed, OPC 97 TM cement mainly contains M1 polymorph whilst OPC 97 cements contain the M1 and M3 polymorph (Fig. 5). In addition, a high amount of C_2S phase of the CP 97 clinker (10.69 wt% - Table 9) is a cause de delay because the C_2S phase is less reactive than the C_3S phase. Previous studies [20, 67] show that the presence of zinc during

clinkerisation had no effect on cement hydration. This is particularly interesting for sediment which often contains the elements such as zinc.

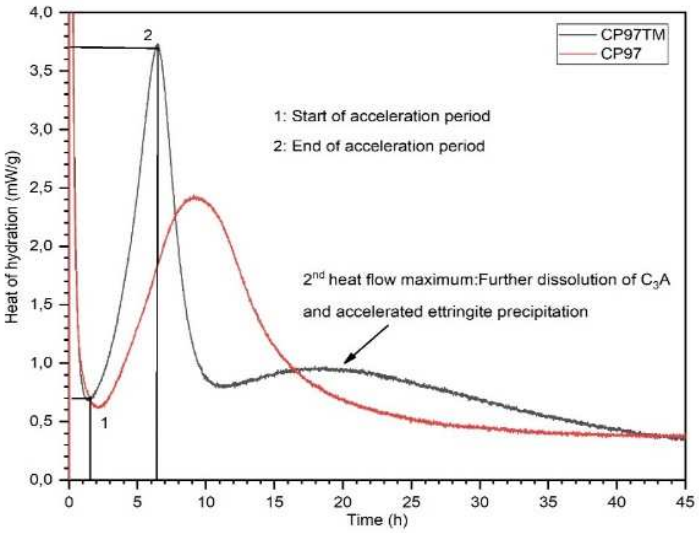

Fig. 13 Heat of hydration of cement pastes (W/C = 0.5)

3.2.3. Degree of hydration of cements

Table 12 shows the theoretical amount of bound water for the two cements for complete hydration. These values depend on the contents of the mineral phases of each cement.

Table 12 Determination of $W_n(\infty)$ from the mineral composition of the cement and the theoretical values of bound water produced for the major phases of the cement for complete hydration

Phase	Coefficient proposed by NIST	Mineral composition of cements (wt%)		Mass of bound water for complete hydration (g/100 g of anhydrous cement)	
		OPC 97 TM	OPC 97	OPC 97 TM	OPC 97
C_3S	0.24	73.96	66.33	17.75	15.92
C_2S	0.21	4.77	10.58	1.00	2.22
C_3A	0.4	5.93	7.51	2.37	3.00
C_4AF	0.37	9.77	10.31	3.62	3.814
Lime	0.33	1.24	0.78	0.408	0.257
Total (%)		95.67	95.51	25.148	25.22

The degree of hydration of the cement pastes after 2 and 28 days of curing using the result from the TGA analysis is shown in Fig. 14.

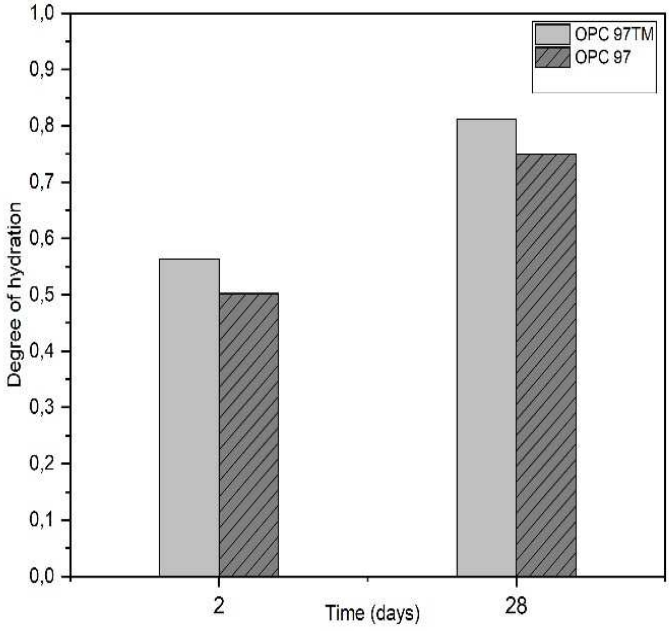

Fig. 14 Degree of hydration of cement pastes (W/C = 0.5)

The measurement result shows that the OPC 97 possesses hydration behavior similar to the OPC 97 TM cement because the degree of hydration of the two cement pastes increases over time of hydration. The degree of hydration of OPC 97 cement reaches 0.51 after 2 days and 0.76 after 28 days. These values are comparable to those of the commercial cement [56]. However, OPC 97 TM cement has the higher degree of hydration than the OPC 97 cement at early ages as well as long term. This is in accordance with that of the calorimetry measurement. In addition, the $Ca(OH)_2$ content formed during cement paste hydration was also measured by TGA analysis. Table 13 presents the $Ca(OH)_2$/initial cement mass ratio of the two cement pastes over time of hydration.

Table 13 $Ca(OH)_2$/initial cement mass ratio over time of hydration

Time (days)	OPC 97 TM	OPC 97
2 days	20.15%	16.31%
28 days	29.04%	25.33%

The result shows that the Ca(OH)2 content formed by the OPC 97 cement paste is lower than that formed by the OPC 97 TM cement paste. The difference is due to the lower content of the C3S phase of OPC 97 cement compared to OPC 97 TM cement. It should be noted that for Portland cement, a low content of Ca(OH)2 corresponds to a low content of C-S-H phase.

The evolution of the mineral phases of hydrated cement paste over time of hydration is presented in Fig. 15 and Fig. 16. The result clearly shows a decrease of anhydrous phases as well as the formation of hydrate phases such as portlandite and ettringite (Aft). However, the presence of C-S-H phase is not identified in the XRD pattern due to its amorphous nature. In conclusion, the substitution rate of the sediment in the raw meal does not modify the mineralogical assemblage of the hydrated cement pastes.

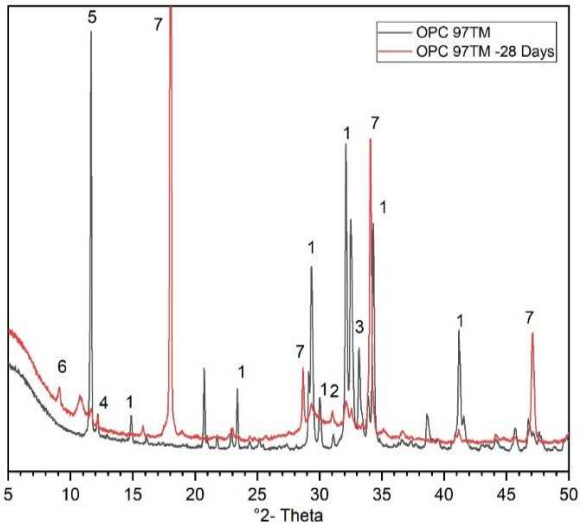

Fig. 15 X-ray diffraction (XRD) of OPC 97 TM cement paste over time of hydration (1: C_3S, 2: C_2S, 3: C_3A, 4: C_4AF, 5: Gypsum, 6: Ettringite (Aft), 7: Portlandite)

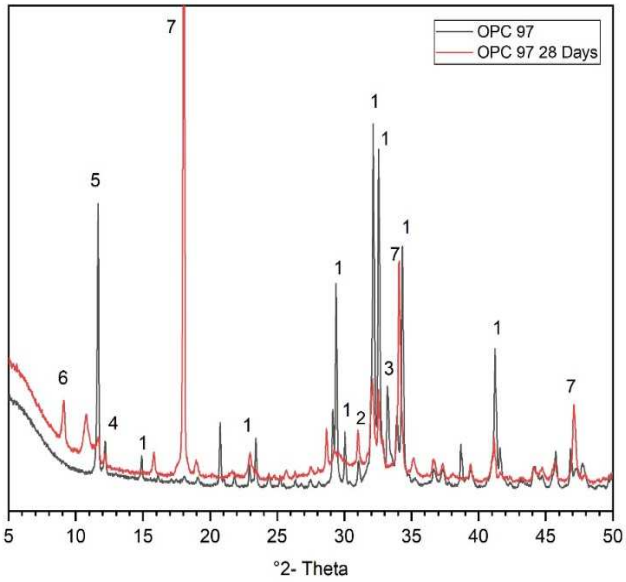

Fig. 16 X-ray diffraction (XRD) of OPC 97 cement paste over time of hydration (1: C_3S, 2: C_2S, 3: C_3A, 4: C_4AF, 5: Gypsum, 6: Ettringite (Aft), 7: Portlandite)

3.2.4. Mechanical performances

Fig. 17 represents the compressive strength of cement pastes after 2, 15 and 28 days of hydration. This choice allows us to study the behavior of resistance development of hydrate cement paste between early ages (2 days) and long term. The development of compressive strength over time was observed in both cement pastes. This is due to the anhydrous cement hydration reaction to form hydrates such as C-S-H phase, which is the origin of the mechanical resistance in the cementitious material. This result also in in accordance with XRD result and degree of hydration result. However, OPC 97 TM cement shows higher compressive strength than the OPC 97 cements at an early ages (2 days) and long term (15 and 28 days). This difference in the compressive strength of the cement pastes could be explained by:

- The retardation effect of the hydration of C_3S observed by the isothermal calorimetry of OPC 97 cement compared to OPC 97 TM cement (Fig. 13) at an early age.
- The C_3S/C_2S ratio of OPC 97 TM cement is higher than that of OPC 97 cement (15.5 and 6.25 for OPC 97 TM, OPC 97 respectively). Knowing that the C_3S reactivity is much higher than that of C_2S phase, this allows to quickly forming the C-S-H phase in the cement paste during hydration.
- The presence of alkali in OPC 97 cement could also have a retardation effect on the hydration and influencing the compressive strength [69].
- After 15 days of hydration, the development of mechanical resistance in the two cement pastes slowed down, in particular in the case of OPC 97 cement which has a high content of C_2S showing slow hydration behavior.

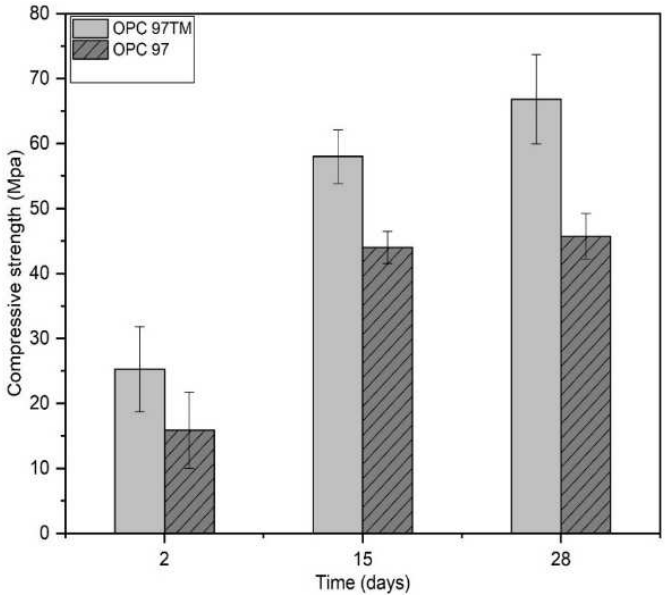

Fig. 17 Compressive strength of cement pastes (W/C = 0.5) after 2, 15 and 28 days of hydration

3.3. NUMERICAL MODELING OF CEMENT HYDRATION

The hydration of the OPC 97 TM and OPC 97 cement was numerically modeled using the CEMHYD3D code. The characteristics of the two cements such as the particle size distribution, the mineral composition were used as the input data to build a numerical cement into the CEMHYD3D code before numerical modeling.

3.3.1. Particle size distribution of cements

The particle size distribution of the OPC 97 TM and OPC 97 cement was measured using the laser particle analyzer COULTER LS 13 320 type. Tables 14 - 15 present the experimental and numerical measurement result of the OPC 97 TM and OPC 97 cements respectively. The result shows that the particle size distribution of the cements used in the CEMHYD3D code is comparable to that of experimental result. This is very important to assume the hydration behavior of cement modeled in the CEMHYD3D code. Indeed, a finer granularity of the cement leads to an acceleration of the hydration kinetics [70].

522 **Table 14** Particle size distribution of OPC 97 TM cement (Experimental and numerical result)

Diameter of particles (μm)	Mass fraction (%) (Exp)	Mass fraction (%) (CEMHYD3D)
1	12.805	12.236
3	4.056	3.874
5	6.023	5.756
7	6.443	6.176
9	6.163	5.909
11	5.662	5.328
13	5.127	4.898
15	4.644	4.611
17	4.259	3.944
19	3.982	3.805
21	3.736	3.820
23	3.490	3.297
25	3.241	2.116
29	5.808	6.639
33	7.257	4.854
37	4.199	6.886
49	10.860	12.851
73	2.250	3.000
Total (%)	100.00	100

523

524 **Table 15** Particle size distribution of OPC 97 cement (Experimental and numerical result)

Diameter of particles (μm)	Mass fraction (%) (Exp)	Mass fraction (%) (CEMHYD3D)
1	11.3487	10.9460
3	3.8930	3.7573
5	5.9458	5.7252
7	7.0075	6.7446
9	7.2094	6.9749
11	6.9718	6.7212
13	6.4481	6.1794
15	5.8153	5.5849

17	5.1927	5.3073
19	4.6175	4.8009
21	4.0419	3.8550
23	3.5097	3.3277
25	3.0766	2.1353
29	5.2911	6.7007
33	6.7252	4.8991
37	3.9203	6.9499
41	6.5334	6.3905
53	1.6881	3.01
57	0.7630	-
Total (%)	99.9993	100.0000

3.3.2. Mineral composition of OPC 97 TM and OPC 97 cement

The CEMHYD3D code uses the volume fraction of mineral phases as input data to build a 3D – microstructure of cement. Therefore, the mineral composition of the cement presented in the Table 12 must be converted into the volume proportion using the densities values of the mineral phases proposed by NIST [71]. Table 16 shows the experimental and numerical result of the mineral composition (volume fraction) of two cements OPC 97 TM and OPC 97 as well as the W/C ratio used. The result demonstrated a good coherence between the experimental and numerical result on the proportion of the phases as well as the W/C ratio. This is very important to assume the precision of the numerical result.

Table 16 Volume fraction of cements OPC 97 TM and OPC 97 (Experimental and numerical result)

Phases	OPC 97 TM cement			OPC 97 cement		
	Exp (%)	CEMHYD3D code		Exp (%)	CEMHYD3D code	
		Pixels	%Volume		Pixels	%Volume
C_3S	74.693	289811	74.617209	66.64	257381	66.267505
C_2S	4.719	18378	4.7317564	10.41	39609	10.198071
C_3A	6.344	24902	6.411481	8	30572	7.8713275
C_4AF	8.492	32944	8.4820429	8.91	34026	8.7606238
Gypsum	5.75	22362	5.757511	6.04	23235	5.982281
Total (%)	99.998	388397	100	100	384823	99.0798
W/C	0.5	0.4999		0.5	0.5	

3.3.3. Determination of the β value in the CEMHYD3D code

In order to determine the β value in the CEMHYD3D code, the values of the degree of hydration of OPC 97 TM and OPC 97 cement pastes at 2 days of hydration measured by TGA analysis were used as the calibration values. In fact, we run a simulation of 1000 cycles with any β value, then we look for the value of the number of cycles that

allows to reach a degree of hydration corresponding to the experimental value of the degree of hydration at 2 days.

The β value is determined according to Eq(15) and Eq(16) equations with the cycle number values previously found. In our case, the β values are equal to 0.00008742 for OPC 97 TM cement and equal to 0.00011186 for OPC 97 cement.

3.3.4. Results of the numerical modeling of cement hydration in the CEMHYD3D code

The hydration of the two cements (OPC 97 TM and OPC 97) was numerically modeled in the code CEMHYD3D at a constant temperature of 20 °C and in the 100% relative humidity, which are similar with the experimental hydration conditions. The modeling results are presented in the following figures and compared with the experimental results to assess the reliability of the CEMHYD3D code in this study.

a) Degree of hydration of cement pastes

Fig. 18 shows the degree of hydration estimated by the CEMHYD3D code comparing with the experimental values measured by the TGA analysis at 2 and 28 days of hydration. A good consistency between the numerical and experimental values was observed. The result in the CEMHYD3D code also showed a higher degree of hydration of OPC 97 TM cement compared to OPC 97 cement at early ages and long term. This is in accordance with previous experimental results.

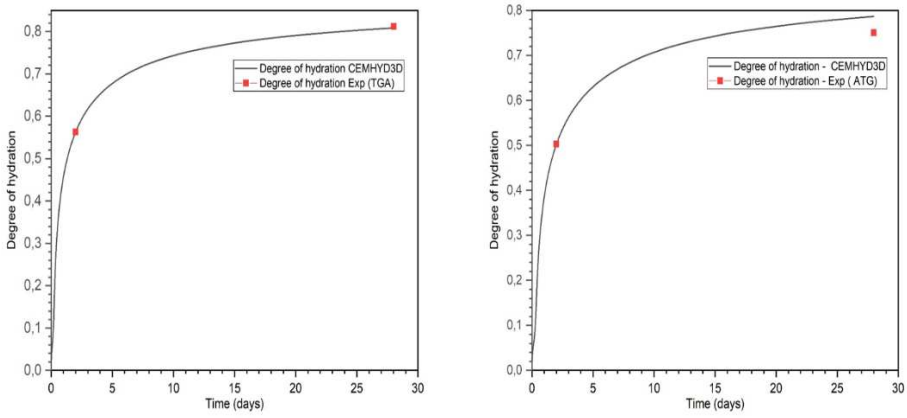

Fig. 18 Degree of hydration of OPC 97 TM (left) and OPC 97 (right) cements (Experimental and numerical result)

Fig. 19 shows the microstructure of cement paste generated from the CEMHYD3D code at the initial state (t = 0) and after 28 days of hydration. This result is very interesting because:

- At the initial state, all the mineral phases of the two cements are present. The size of the anhydrous cement grains is in accordance with the experimental result.
- After 28 days of hydration, the hydrate formation such as C-S-H phase, $Ca(OH)_2$ and the consumption of anhydrous cement grains were also observed. The result shows the influence of anhydrous cement grains size on reactivity during hydration.
- The microstructure generated from the CEMHYD3D code is comparable to that observed by SEM analysis in previous studies [20, 43].

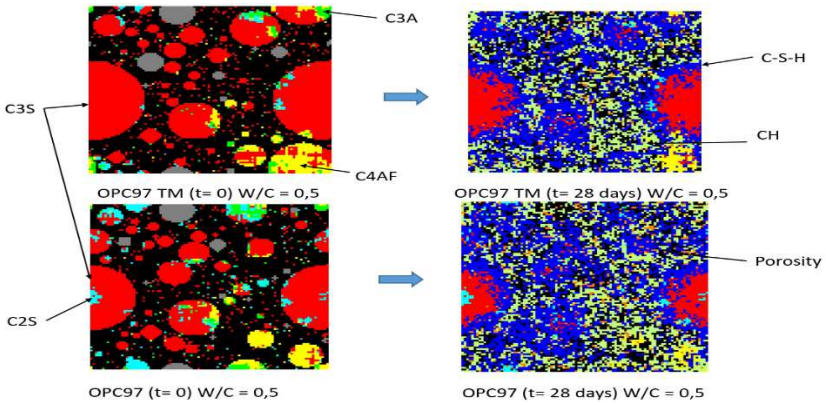

Fig. 19 Microstructure generated in the CEMHYD3D code of OPC 97 TM and OPC 97 cements in the initial state (left) and after 28 days of hydration

b) Compressive strength of cement pastes

The CEMHYD3D code uses Eq(12) equation to estimate the compressive strength of cement paste over time of hydration. The numerical and experimental result of the compressive strength is presented in Fig. 20. The compressive strength estimated by the CEMHYD3D code is in accordance with the experimental results for the two cement pastes. This result confirms that the development behavior of mechanical resistance of the two cement is similar.

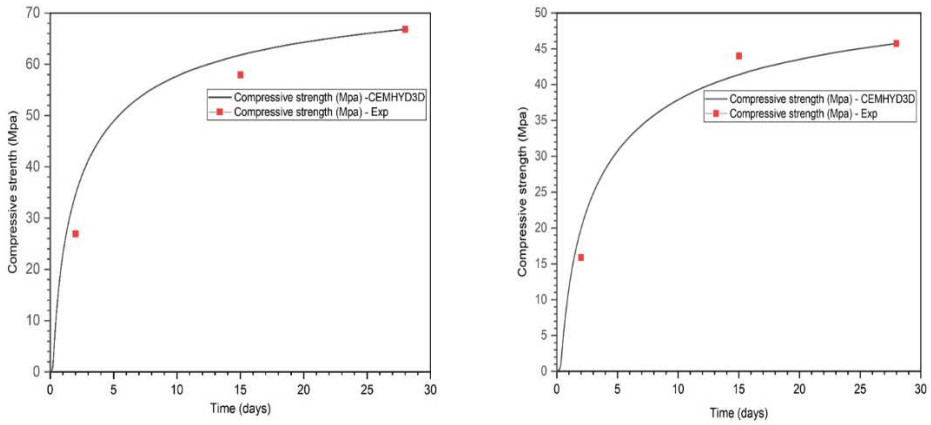

Fig. 20 Numerical and experimental result of the compressive strength of OPC 97 TM (left) and OPC 97 (right) cements

c) Ca(OH)2 quantification in the CEMHYD3D code

Because the $Ca(OH)_2$ phase is a data which can be determined using the TGA analysis, we chose to compare the numerical and experimental quantity of this hydrate to evaluate the reliability of the CEMHYD3D code in our study. CEMHYD3D code presented the evolution of $Ca(OH)_2$ volume over time of hydration, a $Ca(OH)_2$ density value equal of 2.24 (g/cm^3) is used to convert from volume fraction to mass fraction. Fig. 21 shows the $Ca(OH)_2$/ initial cement mass ratio of two cement pastes over the time of hydration.

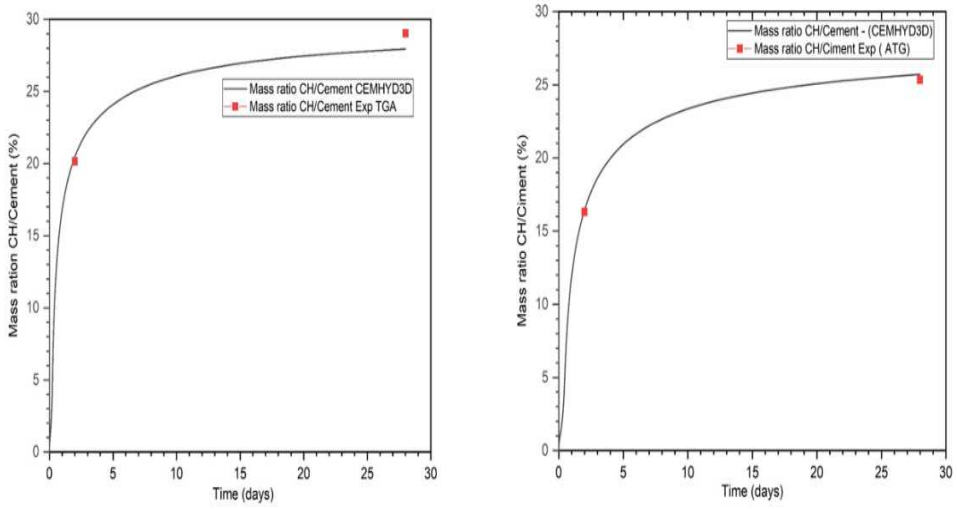

Fig. 21 CH/initial cement mass ratio of OPC 97 TM (left) and OPC 97 (right) cement paste

From the result in Fig. 21, we note that the CEHDYD3D code shows a good consistency with the experimental results for the two cement pastes. In addition, the CEMHYD3D code also makes it possible to monitor the evolution of the anhydrous phases as well as the hydrates over time of hydration. This is interesting because it is difficult to follow the evolution of phases by experimental analysis, for example C-S-H phase. This phase is responsible for the development of mechanical resistance in the cementitious materials. Following the evolution of C-S-H could help understand the development of mechanical strength. In this study, we present the numerical result of the evolution of C-S-H over time of hydration in the CEMHYD3D code (Fig. 22).

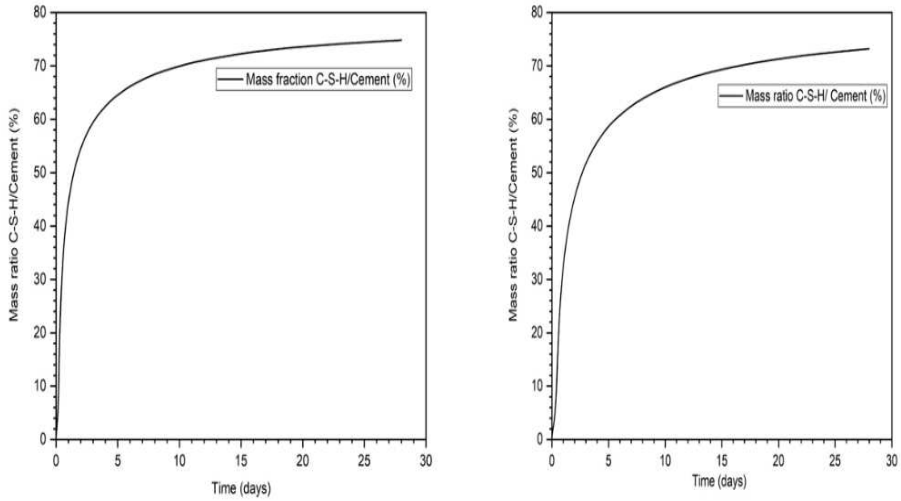

Fig. 22 C-S-H/Initial cement mass ratio measured by CEMHYD3D code for OPC 97 TM (left) and OPC 97 (right) cement pastes over time of hydration

From the result of the C-S-H/initial cement mass ration, we can extract the following conclusions:

- OPC 97TM has a higher C-S-H/ initial cement mass ratio than OPC 97 cement at early ages (2 days). This may explain the higher mechanical resistance development of OPC 97TM compared to OPC 97.
- At 28 days of hydration, this ratio is relatively similar for the two cements, however the compressive strength of the OPC 97TM cement is higher than that of the OPC 97 cement. This may be due to the presence of the minor elements integrated into C-S-H phase which influence mechanical performance.

4. CONCLUSION

The objective of this study is to recycle the maximum amount of the NSL sediment as a raw material in the cement production at laboratory. The following principal results are obtained:

- The NSL sediment contains the 4 principal oxides such as CaO SiO_2, Al_2O_3 and Fe_2O_3 which needs to produce the Portland cement.

- A substitution rate of 31 wt% of NSL sediment can be recycle in the raw meal to produce Portland cement.
- In all produced clinkers (the reference clinker and the clinker made from the substitution of sediment), the 4 principal crystalline phases of an ordinary Portland cement such as C_3S, C_2S, C_3A and C_4AF are identified. The XRD pattern and SEM – EDS analysis indicate that the substitution of the sediment promotes the formation of M3 polymorph in C_3S phase and an orthorhombic polymorph in C_3A phase due to the presence of minor oxides such as MgO, Na_2O.
- The result of free lime content quantification and the identification of the crystalline phases of the clinkers show that the cooling process used in this study did not cause a negative effect such as the decomposition of alite.
- The typical form of alite and belite was also identified. The presence of SO_3 in CP97 clinkers promotes the formation of larger crystals of alite than those in the reference clinker CP 97 TM.
- The atomic ratio of the major elements in the main phases of the two clinkers measured from the SEM-EDS analysis is higher than the theoretical values. However, the ratio of C_2S, C_3A, C_4AF phases are relatively similar, while the ratio in C_3S phase of clinker made from the substitution of the sediment is higher than that of reference clinker. The substitution of sediment seems to have more effect on the C_3S formation than other phases in the clinker.
- The two cements show similar hydration behavior similar. However, the mechanical performance of cement decreases with the substitution rate of sediment. This can be explained by the formation of the M3 polymorph of C_3S in the clinker-based sediment which is less reactive than the M1 polymorph.
- The zinc presence in the sediment does not modify the C_3A formation in the clinker. The zinc is present in all phases except in the C_2S phase. In addition, the presence of zinc in clinker phases does not influence on the hydration behavior of cement. This is very interesting because the sediment often contains elements such as zinc.
- The CEMHYD3D code was used to simulate the hydration of OPC 97 TM and OPC 97 cement paste. The numerical and experimental results are quite consistent. The modeling result confirms the hydration behavior of cement produced at laboratory. This code also allows us to visually follow the evolution of all phases over time of hydration. This is interesting because the hydration of the cement is a complex process and difficult to follow all the evolutions by the experimental analysis. In addition, based on the numerical modeling result generated from the CEMHYD3D code, several studies of the microstructure can be investigated as leaching coupling with other computer code.

Funding

No applicable

Declarations of Competing Interest

The authors declare that they have no known competing financial interests or personal relationships that could have appeared to influence the work reported in this paper.

Availability of data and material:

We confirm that all results are available in the database. If necessary, please contact us at the address: duc.chinh.chu@imt-lille-douai.fr

Code availability: CEMHYD3D: A Three-Dimensional Cement Hydration and Microstructure Development Modelling Package. Version 2.0 | NIST

Acknowlegments

The authors wish to acknowledge the SEDICIM project and the FEDER funds.

Reference

1. INSEE: https://www.insee.fr/fr/statistiques/3589283
2. Kajaste, R., Hurme, M.: Cement Industry Greenhouse Gas Emissions - Management Options and Abatement Cost. J. Clean. Prod. 112, 4041–4052 (2015)
3. Ademe: Déchet, Chiffres-clés. (2015)
4. Pan, J.R., Huang, C., Kuo, J.J., Lin, S.H.: Recycling MSWI bottom and fly ash as raw materials for Portland cement. Waste Manag. 28, 1113–1118 (2008). https://doi.org/10.1016/j.wasman.2007.04.009
5. Ferreira, C., Ribeiro, A., Ottosen, L.: Possible applications for municipal solid waste fly ash. J. Hazard. Mater. 96, 201–216 (2003). https://doi.org/10.1016/S0304-3894(02)00201-7
6. Mukiza, E., Zhang, L.L., Liu, X., Zhang, N.: Utilization of red mud in road base and subgrade materials: A

review. Resour. Conserv. Recycl. 141, 187–199 (2019). https://doi.org/10.1016/j.resconrec.2018.10.031
7. De Larrard, F., Colina, H.: Le béton recyclé. (2018)
8. Chen, G., Lee, H., Young, K.L., Yue, P.L., Wong, A., Tao, T., Choi, K.K.: Glass recycling in cement production-an innovative approach. Waste Manag. 22, 747–753 (2002). https://doi.org/10.1016/S0956-053X(02)00047-8
9. Renaut, M.: Calcination des déchets industriels : synthèse de ciment et stabilisation / solidification des résidus de combustion - Thèse de doctorat, (2017)
10. Dubois, V.: Etude du comportement physico-mécanique et caractérisation environnementale des sédiments marins – Valorisation en technique routière - Thèse de doctorat, (2006)
11. Scordia, P.: Caractérisation et valorisation de sédiments fluviaux pollués et traités dans les matériaux routiers, (2008)
12. Tribout, C.: Valorisation de sédiments traités en techniques routières : contribution à la mise en place d'un protocole d'acceptabilité. Thèse de doctorant de l'Université Toulouse III, (2010)
13. Miraoui M.: Mise en œuvre d'une démarche de prétraitement et de traitement des sédiments de dragage en vue d'une valorisation dans le génie civil - Thèse de doctorat
14. M.Dia: Traitement et valorisation de sédiments de dragage phosphatés en technique routière - Thèse de doctorat, (2013)
15. S.Brakni: Première approche vers une valorisation de granulats artificiels à base de sédiments de dragage - Thèse de doctorat, (2008)
16. Amar, M.: Étude expérimentale et numérique de la valorisaion des sédiments de dragage dans les matrices cimentaires - Thèse de doctorat, (2017)
17. Zhao, Z., Benzerzour, M., Abriak, N.E., Damidot, D., Courard, L., Wang, D.: Use of uncontaminated marine sediments in mortar and concrete by partial substitution of cement. Cem. Concr. Compos. 93, 155–162 (2018). https://doi.org/10.1016/j.cemconcomp.2018.07.010
18. Taylor HFW: Cement chemistry. (1997)
19. Dalton, J.L., Gardner, K.H., Seager, T.P., Weimer, M.L., Spear, J.C.M., Magee, B.J.: Properties of Portland cement made from contaminated sediments. Resour. Conserv. Recycl. 41, 227–241 (2004). https://doi.org/10.1016/j.resconrec.2003.10.003
20. Aouad, G., Laboudigue, A., Gineys, N., Abriak, N.E.: Dredged sediments used as novel supply of raw material to produce Portland cement clinker. Cem. Concr. Compos. 34, 788–793 (2012). https://doi.org/10.1016/j.cemconcomp.2012.02.008
21. Faure, A., Smith, A., Coudray, C., Anger, B., Colina, H., Moulin, I., Thery, F.: Ability of Two Dam Fine-Grained Sediments to be Used in Cement Industry as Raw Material for Clinker Production and as Pozzolanic Additional Constituent of Portland-Composite Cement. Waste and Biomass Valorization. 8, 2141–2163 (2017). https://doi.org/10.1007/s12649-017-9870-8
22. Faure, A., Coudray, C., Anger, B., Moulin, I., Colina, H., Izoret, L., Théry, F., Smith, A.: Beneficial reuse of dam fine sediments as clinker raw material. Constr. Build. Mater. 218, 365–384 (2019). https://doi.org/10.1016/j.conbuildmat.2019.05.047
23. XP 94- 047 : Détermination de la teneur pondérale en matières organiques d'un matériau - Méthode par calcination. (1998)
24. Association Française de Normalisation (AFNOR): NF EN 1097-7 : Détermination de la masse volumique absolue du filler - Méthode au pycnomètre. (2008)
25. Association Française de Normalisation (AFNOR): NF EN 196-6 : Méthodes d'essai des ciments - Détermination de la finesse. (2018)
26. NF EN 12457-2. Leaching-Compliance Test for LeachingofGranular Waste Materials and SludgesPart 2: One Stage Batch Test at a Liquid to Solid Ratio of10 l/kgfor Materials with Particle Size Below 4 mm (without or with Size Reduction); BSI: London, UK, 2002.
27. Centre d'information sur le ciment et ses appications: Ciments et Bétons.
28. ANGER, B., THERY, F., LEVACHER, D.: Caractérisation des sédiments fins des retenues hydroélectriques en vue d'une pré-orientation vers des filières de valorisation matière. 97–102 (2015). https://doi.org/10.5150/cmcm.2015.020
29. Dia, M., Ramaroson, J., Nzihou, A., Zentar, R., Abriak, N.E., Depelsenaire, G., Germeau, A.: Effect of

chemical and thermal treatment on the geotechnical properties of dredged sediment. Procedia Eng. 83, 159–169 (2014). https://doi.org/10.1016/j.proeng.2014.09.034
30. Teklay, A., Yin, C., Rosendahl, L., Køhler, L.L.: Experimental and modeling study of flash calcination of kaolinite rich clay particles in a gas suspension calciner. Appl. Clay Sci. 103, 10–19 (2015). https://doi.org/10.1016/j.clay.2014.11.003
31. Lea: Lea's chemistry of cement and concrete. Elsevier. (2003)
32. G.K.Moir: Advanced Concrete Techbology. (2003)
33. G.K.Moir; Mineralised high alite cement. World Cem. 13, 374 (1982)
34. F.W.Locher: Cement principles of production and use. (2006)
35. Lawrence, C.D.: The Constitution and Specification of Portland Cements. (2004)
36. Neville, A.: Propriétés des Bétons, édition Eyrolles, Translated by CRIB. (2000)
37. Hill, L., Fulvio, T.: Manufacturing solutions for concrete performance, World cement.
38. Baron, J., Ollivier, J.-P.: Les Bétons. (1997)
39. Zayed, A.: Effect of sulfur trioxide content on concrete structures using Florida Materials, Research report, University of south Florida. (2004)
40. Association Française de Normalisation (AFNOR): NF EN 197-1: Composition, spécifications et critères de conformité des ciment courant.
41. Faure, A.: Capacité d ' un sédiment à se substituer à la fraction argileuse de la matière première de l ' industrie des liants hydrauliques - Thèse de doctorat, (2017)
42. Kleib, J., Aouad, G., Khalil, N., Zakhour, M.: Incorporation of zinc in calcium sulfoaluminate cement clinker. Adv. Cem. Res. 1–7 (2020). https://doi.org/10.1680/jadcr.19.00125
43. Chu, D.C., Kleib, J., Amar, M., Benzerzour, M., Abriak, N.-E.: Determination of the degree of hydration of Portland cement using three different approaches: Scanning electron microscopy (SEM-BSE) and Thermogravimetric analysis (TGA). Case Stud. Constr. Mater. 15, e00754 (2021). https://doi.org/10.1016/j.cscm.2021.e00754
44. Patel, R.G., Killoh, D.C., Parrott, L.J., Gutteridge, W.A.: Influence of curing at different relative humidities upon compound reactions and porosity in Portland cement paste. Mater. Struct. 21, 192–197 (1988). https://doi.org/10.1007/BF02473055
45. Snyder, K.A., Bentz, D.P.: Suspended hydration and loss of freezable water in cement pastes exposed to 90% relative humidity. Cem. Concr. Res. 34, 2045–2056 (2004). https://doi.org/10.1016/j.cemconres.2004.03.007
46. NIST: Technical Note VCCTL-01.
47. Kleib, J., Aouad, G., Abriak, N.E., Benzerzour, M.: Production of Portland cement clinker from French Municipal Solid Waste Incineration Bottom Ash. Case Stud. Constr. Mater. 15, e00629 (2021). https://doi.org/10.1016/j.cscm.2021.e00629
48. T. Knudsen: The dispersion model for hydration of portland cement I. General concepts. Cement and Concrete Research, 14, pp.622–630 (1984).
49. Mounanga, P., Khelidj, A., Loukili, A., Mounanga, P., Khelidj, A., Loukili, A., Predicting, V.B.: Predicting Ca (OH) 2 content and chemical shrinkage of hydrating cement pastes using analytical approach To cite this version : HAL Id : hal-01007190. (2004)
50. B. Lothenbach, F. Winnefeld, C. Alder, E. Wieland, P. Lunk: Effect of temperature on the pore solution, microstructure and hydration products of Portland cement pastes. Cement and Concrete Research, 37, pp.483–491 (2007).
51. van Breugel, K.: Numerical simulation of hydration and microstructural development in hardening cement-based materials (I) theory. Cem. Concr. Res. 25, 319–331 (1995). https://doi.org/10.1016/0008-8846(95)00017-8
52. Bentz, D.P.: Incorporation of Fly Ash into a 3-D Cement Hydration Microstructure Model Nistir 6050. (1997)
53. Bentz, D.P.: Modeling the influence of limestone filler on cement hydration using CEMHYD3D. Cem. Concr. Compos. 28, 124–129 (2006). https://doi.org/10.1016/j.cemconcomp.2005.10.006
54. Kamali, S., Moranville, M., Garboczi, E., Prené, S., Gérard, B.: Hydrate dissolution influence on the Young's modulus of cement pastes. Proc. 5th Int. Conf. Fract. Mech. Concr. Concr. Struct. 12–16 (2004)
55. NIST: Guide to using CEMHYD3D Version 3.0.

56. Bresciani, C.: Simulation numérique de l ’ hydratation et du développement des propriétés physiques et mécaniques d ’ une pâte de ciment afin de sélectionner de nouveaux ajouts minéraux., (2009)
57. Bentz, D.P.: Guide to Using CEMHYD3D: A Three-Dimensional Cement Hydration and Microstructure Development Modelling Package. (1997)
58. Li, T., Xiao, J., Zhu, C.: Hydration process modeling of ITZ between new and old cement paste. Constr. Build. Mater. 109, 120–127 (2016). https://doi.org/10.1016/j.conbuildmat.2016.01.053
59. Kamali, S., Bernard, F., Damidot, D.: Modélisation multi-échelles de la lixiviation des mortiers : effet sur les caractéristiques mécaniques. 7–12 (2005)
60. Faure, A.: Capacité d ’ un sédiment à se substituer à la fraction argileuse de la matière première de l ’ industrie des liants hydrauliques - Thèse de doctorat, (2017)
61. Gineys, N., Aouad, G., Sorrentino, F., Damidot, D.: Incorporation of trace elements in Portland cement clinker: Thresholds limits for Cu, Ni, Sn or Zn. Cem. Concr. Res. 41, 1177–1184 (2011). https://doi.org/10.1016/j.cemconres.2011.07.006
62. Tang, S., Wang, Y., Geng, Z., Xu, X., Yu, W., A, H., Chen, J.: Structure, fractality, mechanics and durability of calcium silicate hydrates. Fractal Fract. 5, (2021). https://doi.org/10.3390/fractalfract5020047
63. Wang, L., Jin, M., Zhou, S., Tang, S., Lu, X.: Investigation of microstructure of C-S-H and micro-mechanics of cement pastes under NH4NO3 dissolution by 29Si MAS NMR and microhardness. Measurement. 185, 110019 (2021). https://doi.org/10.1016/j.measurement.2021.110019
64. Bye, G.C.: Portland cement: Composition, production and properties. (1999)
65. Clark, M.: Petcoke and Nodulisation. Int. Cem. Rev. 39 (2003)
66. Berthomier, M.: Etude de la lixiviation de l’aluminium de matériaux cimentaires à base de CEM III utilisés dans les canalisations d’eau potable : approche expérimentale et numérique. (2020)
67. Gineys, N., Aouad, G., Damidot, D.: Managing trace elements in Portland cement - Part II: Comparison of two methods to incorporate Zn in a cement. Cem. Concr. Compos. 33, 629–636 (2011). https://doi.org/10.1016/j.cemconcomp.2011.03.008
68. HORNAIN H.: SUR LA REPARTITION DES ELEMENTS DE TRANSITION ET LEUR INFLUENCE SUR QUELQUES PROPRIETES DU CLINKER ET DU CIMENT Réf. ATILH n°04005. CIMENTS BETONS, Rev. DES Mater. Constr.
69. Witzleben, S.T.: Acceleration of Portland cement with lithium, sodium and potassium silicates and hydroxides. Mater. Chem. Phys. 243, 122608 (2020). https://doi.org/10.1016/j.matchemphys.2019.122608
70. Bentz, D.P.: Three-dimensional computer simulation of portland cement hydration and microstructure development. J. Am. Ceram. Soc. 80, 3–21 (1997). https://doi.org/10.1111/j.1151-2916.1997.tb02785.x
71. Bentz, D.P.: CEMHYD3D : A Three-Dimensional Cement hydratation and Microstructure Development Modelling Package Version 2.0.